Vis Comput
DOI 10.1007/s00371-012-0673-4

ORIGINAL ARTICLE

Rendering realistic spectral bokeh due to lens stops and aberrations

Jiaze Wu · Changwen Zheng · Xiaohui Hu · Fanjiang Xu

© Springer-Verlag 2012

Abstract Creating bokeh effect in synthesized images can improve photorealism and emphasize interesting subjects. Therefore, we present a novel method for rendering realistic bokeh effects, especially chromatic effects, which are absent for existing methods. This new method refers to two key techniques: an accurate dispersive lens model and an efficient spectral rendering scheme. This lens model is implemented based on optical data of real lenses and considers wavelength dependency of physical lenses by introducing a sequential dispersive ray tracing algorithm inside this model. This spectral rendering scheme is proposed to support rendering of lens dispersion and integration between this new model and bidirectional ray tracing. The rendering experiments demonstrate that our method is able to simulate realistic spectral bokeh effects caused by lens stops and aberrations, especially chromatic aberration, and feature high rendering efficiency.

Keywords Bokeh effect · Lens stops · Lens aberrations · Dispersive lens model · Spectral rendering

1 Introduction

Bokeh effect means the blur in out of focus (OOF) regions of an image produced by lenses of finite aperture, and, more exactly, refers to aesthetic quality of blur appearance, including size, shape, and light intensity distribution of circle of confusion (COC). Bokeh effect is similar to depth of field (DOF) effect because both kinds of effects mean blur of the OOF background or foreground. However, DOF effect is merely related to the blur amount, while bokeh effect lays more stress on the blur appearance of an OOF point, especially for small light sources and specular highlights in OOF areas of a photo [1, 20], illustrated in Fig. 1. Adding accurate bokeh effect into a synthesized image can dramatically enhance image photorealism and improve depth perception and user comprehension. In addition, generation of artistic bokeh is also another interesting application. A few of approaches have been proposed to simulate this kind of effect in recent years, but hardly produce compellent and accurate results due to their incompetence at accurately modeling the optical properties of complex lenses or lack of accurate scene information.

In this paper, a novel spectral bokeh rendering method, which incorporates both accurate modeling of complex lens system and accurate scene information, is proposed. Our method firstly presents a new physically-based dispersive lens model with multiple aspects of new features, such as lens stops, real glass data, and dispersive ray tracing inside the model. By this new model, various optical properties, especially spectral properties, of physical lenses are able to be accurately modeled. We also propose a serial of efficient spectral rendering techniques, including an efficient spectral sampling technique, a hybrid scheme for dealing with the dispersion, and a modified bidirectional ray tracing approach for integrating our model, which are combined with this model to achieve generation of realistic bokeh effect, especially various colorful bokeh.

J. Wu (✉) · C. Zheng · X. Hu · F. Xu
National Key Laboratory of Integrated Information System Technology, Institute of Software, Chinese Academy of Sciences, Beijing, China
e-mail: wujiaze05@gmail.com

J. Wu
Graduate University of Chinese Academy of Sciences, Beijing, China

Published online: 09 February 2012

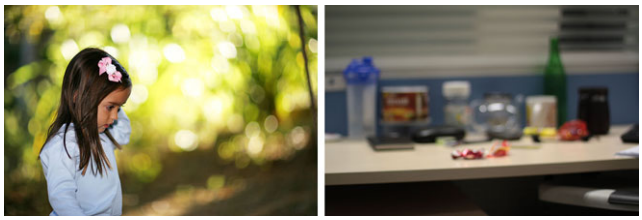

Fig. 1 Photographs characteristic of bokeh effects. (**a**) The blur shapes are circular in the center of the photo, but become more elliptic when closer to the perimeter [35] (Image courtesy of Paul van Walree [32]); (**b**) The bokehs in the OOF highlights become colorful due to chromatic aberration, photographed by the Cannon EOS 50D with F/1.4

2 Related work

2.1 Bokeh rendering

DOF effect, viewed as a simplified bokeh effect, gains comprehensive attention, and numerous techniques have been proposed for rendering this kind of effect. These algorithms fall into two categories: single-view methods [14, 19, 23] and multi-view methods [8, 17, 26]. The single-view methods depend on post-processing, such as gathering and scattering, of a single-view image to gain very high rendering performance for real-time applications. On the contrary, the multi-view methods, such image accumulation and distributed ray tracing, are capable of simulating more realistic DOF effect at the cost of heavy computation. Based on these methods, many rendering methods for DOF effect are extended to render bokeh effect.

Bokeh effect was first mentioned by Potmesil and Chakravarty [23]. Based on wave theory and the thin lens model, the Lommel function was introduced to represent the light intensity distribution in the COC, but no actual bokeh effect is produced. The gathering-based method was extended by applying a variety of filters with different shapes and intensity distributions to obtain plausible bokeh effects [11, 24]. However, relatively high quality bokeh effect is rather difficult with this method, since bokeh patterns are determined by the scattered pixels from a source image rather than the gathered neighbor pixels [9]. Therefore, the scattering method can simulate more accurate bokeh by exploiting some special techniques, such as texture extension of GPU point sprites [19], composite of a set of simple images describing basic aperture shapes [16], and summed area table [13].

However, these methods above only rely on single image, and hence results are approximate and plausible. Lee et al. [18] simulated bokeh effects due to spherical aberration, based on a layered image-based scene and a simple geometric lens. In spite of gaining high real-time performance, various realistic bokeh effects due to lens stops and multiple kinds of aberrations are unachievable. Buhler et al. [3] used an arbitrary probability density function to represent the intensity distribution within the COC, and combined distributed ray tracing to achieve more accurate effects than the single-view methods, but adapted the thin lens model. Wu et al. [37] simulated realistic bokeh effects dependent on monochromatic aberrations by using a realistic lens model and distributed ray tracing, but the bokeh effects stemming from lens stops and chromatic aberrations are not still taken into account.

2.2 Dispersion modeling

Light dispersion occurs when polychromatic light is split into its spectral components on a refractive material boundary due to the wavelength dependency of the refractive indices in transparent materials. Light dispersion creates a variety of colorful optical effects, which draw great interests from computer graphics aiming at simulating these effects. Some researchers proposed a few approaches, such as spread ray tracing [29, 38] and composite spectral model [27, 28], to model the light dispersion. However, existing approaches are only used to model general light dispersion in a 3D scene, especially rendering of gemstones, but lens dispersion, e.g. chromatic bokeh, is never considered.

3 Lens stops

A lens system typically has many openings, or geometric structures that limit the incident light through the lens system. These structures, generally called stops, may be the edge of a lens or mirror, a ring or other fixture that holds a lens element in place, or may be a special element such as a diaphragm placed in the light path to limit the light through the lens system. Of these stops, the aperture stop is the stop that determines the ray cone angle of a point near the optical axis and the vignetting stop is the stop that limits the ray bundle of a point far from the optical axis. Both stops play an important role in shaping the bokeh. The shape of bokeh appearing near the center of an image is individually determined by the aperture stop but the bokeh existing in the periphery is affected by both the aperture stop and vignetting stops when there are no aberrations in the lens.

3.1 Aperture stop

In optics, the aperture stop is the aperture that most limits the amount of light entering a lens system, and its images in the object space and image space are called the entrance and exit pupils, respectively [6]. In other words, the entrance pupil is the image of the aperture stop as it would be seen if viewed from the axial point on the object; the exit pupil is the image of the aperture stop as it would be seen if viewed from the final image plane. Figure 2 illustrates the optical

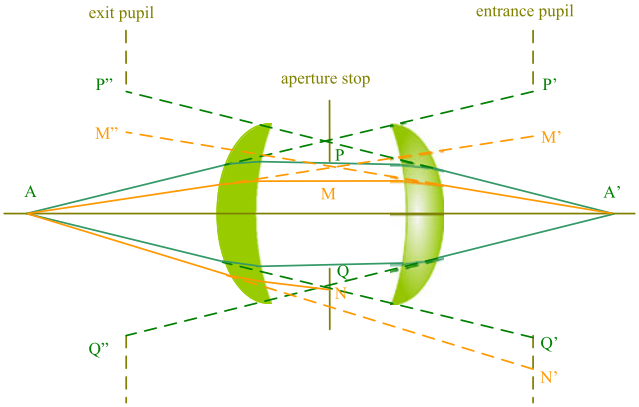

Fig. 2 Optical relationship of the aperture stop, entrance pupil and exit pupil of a doublet

Fig. 3 The shape of the entrance pupil varies with both the aperture size and the angle of incidence. The white openings correspond to the clear aperture for light that reaches the image plane. (Image courtesy of Paul van Walree [33])

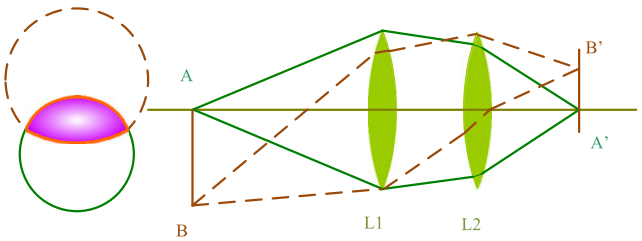

Fig. 4 Basic optical principle of vignetting formation

relationship among the aperture stop (PQ), entrance pupil (P′Q′) and exit pupil (P″Q″).

Based on the optical definitions of the aperture stop, entrance and exit pupils, there is a conjugate relationship among them [6]. More precisely, if a light path starting from an axial point passes through one of them, it would be bound to pass through other ones and eventually the entire lens system. On the contrary, if a light path can not pass through any of them, it cannot also pass through any others.

The aperture stop may be circular, polygonal, or other arbitrary shapes. The aperture stop has a great influence on the appearance of bokeh. It determines the shape of bokeh in the middle of a photo, and influences the shape of bokeh in the edge of a photo. When a lens is stopped down to a value far less than its maximum aperture size (minimum f-number), OOF points are blurred into polygons rather than perfect circles, as shown in Fig. 3. This is most apparent when a lens produces undesirable, hard-edged bokeh and, therefore, some lenses have aperture blades with curved edges to make the aperture more closely approximate a circle rather than a polygon.

3.2 Vignetting stop

When a beam of rays from an off-axis point passes through a lens system, it may be partially blocked by the rims of some elements in the lens system. This optical phenomenon is called vignetting, whose basic optical principle is explained in Fig. 4. The beam of rays emanating from the point B (dashed line) is limited on its lower edge by the lower rim of the lens L1 and on its upper edge by the upper rim of the lens L2. The clear aperture of the lens system when viewed from point B is shown in the left side of Fig. 4. The clear aperture has become the common area of two circles, one (solid line) of which is the clear diameter of L1, and the other (dashed line) the clear diameter of L2's image produced by L1. The white opening of the left bottom lens in Fig. 3 corresponds to the clear aperture affected by vignetting when seen from the semi-field angle. Vignetting gradually and radially reduces the light intensity and changes the bokeh shape in the periphery of the image, and Fig. 1 shows the so-called cat's eye effect due to vignetting.

4 Lens aberrations

Lens aberrations, ubiquitous in lens systems, refer to deviation of the imaging characteristics of a lens system from the perfect predictions by Gaussian optics [2], as illustrated in Fig. 5. Aberrations can fall into two categories: monochromatic and chromatic. Monochromatic aberrations are caused by the geometry of the lens and occur when light is either refracted or reflected. They appear even when only using monochromatic light. Chromatic aberrations are incurred by lens dispersion, the variation of a lens's refractive index with wavelength. They do not appear when monochromatic light is used. Lens aberrations, both monochromatic and chromatic, usually result in blurring of images (Fig. 5(b)) and, therefore, make a important impact on bokeh appearance, including its shape and intensity distribution. In this section,

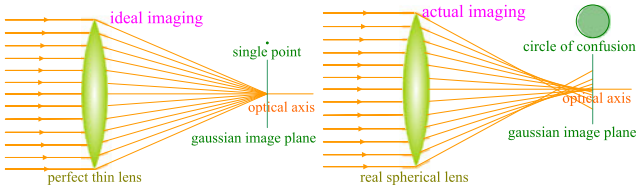

(a) Ideal imaging (b) Actual imaging

Fig. 5 Perfect thin lens produces a single point on Gaussian image plane, but real spherical lens produces a circle of confusion on the image plane

we will present a simple schematic optical explanation on how various kinds of aberrations influence bokeh on images.

4.1 Monochromatic aberrations

The monochromatic aberrations, which have an important impact on the bokeh appearance, include spherical aberration, coma, astigmatism, and field curvature. Spherical aberration determines the light intensity distribution within the COC in the middle of an image. Coma can affect both the shape and light distribution of the COC in the periphery of an image. Astigmatism and field curvature can cause the curved image surface, and elongate the shape of the COC. The more detailed explanations about monochromatic aberrations can be found in previous work [37].

4.2 Chromatic aberrations

In optics, chromatic aberration is the incapability of a lens system to focus different wavelengths of light to the exact same point. It occurs because the refractive materials of lenses have different refractive indices for different wavelengths, and can be regarded as a special kind of dispersion phenomenon inside the lens system. Since the focal length f of a lens is dependent on the refractive index n, different wavelengths of light will be focused on different positions. Chromatic aberration can be both axial (longitudinal), in that different wavelengths are focused at a different distance from the lens, as illustrated in Fig. 6(a); and lateral (transverse), in that different wavelengths are focused at different positions in the focal plane (because the magnification of the lens also varies with wavelength), as illustrated in Fig. 6(b). Chromatic aberration is usually perceived in the form of colored fringes or colored blur along contrasty edges that separate dark and bright parts of an image, especially the colored blur, also called as chromatic bokeh, in the OOF area of the image, as illustrated in Fig. 1.

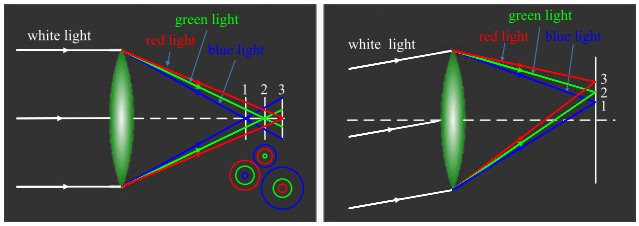

Fig. 6 Chromatic aberration of a single lens. (**a**) The focal length varies with wavelength; (**b**) The magnification varies with wavelength

5 Dispersive lens model

5.1 Dispersive equation

Generally, the refractive index of a lens material, such as glass, plastic and crystalline, non-linearly decreases with increasing wavelength, indicated in Fig. 7. The non-linear wavelength dependency can be described by dispersion equation. Many forms of a dispersion equation exist, but two of them are the most commonly used equations, namely Schott and Sellmeier equations [2, 15], used by Schott, Hoya, and other optical glass manufacturers:

$$\textit{Schott}: \quad n^2(\lambda) = a_0 + a_1\lambda^2 + a_2\lambda^{-2} + a_3\lambda^{-4} + a_4\lambda^{-6} + a_5\lambda^{-8},$$

$$\textit{Sellmeier}: \quad n^2(\lambda) = a_0 + \frac{a_1\lambda^2}{\lambda^2 - b_1} + \frac{a_2\lambda^2}{\lambda^2 - b_2} + \frac{a_3\lambda^2}{\lambda^2 - b_3},$$

where λ is the wavelength expressed in μm, and other constant coefficients are provided by glass manufacturers.

The coefficients of the dispersion equations can be obtained from a variety of formats of glass catalogs provided by glass manufacturers, which are often available from the company websites free of charge. In our paper, we use the AGF file format for our lens model, which are devised and used by the ZEMAX lens design software [39] and becoming a de facto standard in lens design field. The Schott catalog is used as the major option to provide the dispersion data in the following experiments and the Hoya glass catalog is replaced when the glass does not exist in the Schott catalog. While reading the AGF file, we find that the new Schott catalog adopts the Sellmeier equation, but the Hoya catalog still uses the Schott equation.

However, after obtaining these dispersion coefficients, we do not directly use them to compute the refractive index at any wavelength. Instead, we firstly pre-compute the refractive index as a table for a fix set of wavelength in equal internals (usually 1 nm) at the visual spectrum, and then interpolate them to obtain arbitrary refractive index.

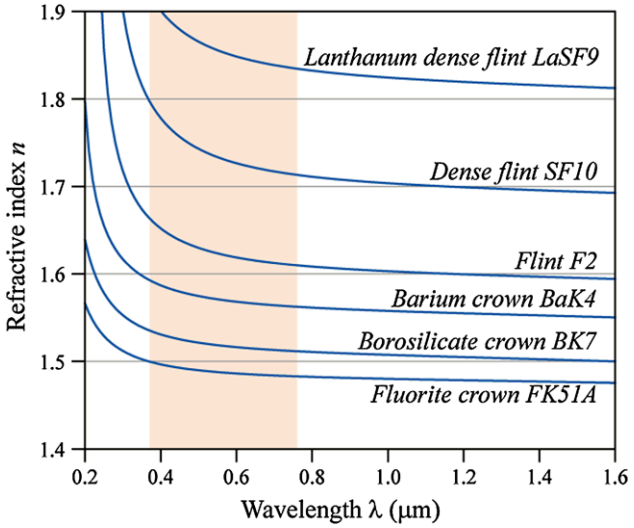

Fig. 7 The refractive index of various lens materials is dependent on wavelength and the wavelengths of visible light are marked in *shallow red* [36]

5.2 Dispersive refraction

When a beam of white light enters into a lens system, dispersive refraction occurs. The law of refraction, also called Snell law, is a formula used to describe the relationship between the angles of incidence and refraction for a monochromatic light. Lens elements are made of transparent materials, such as glass, plastic, and crystalline and, therefore, the law of refraction can be used to describe the interaction of light with a lens system. Wu et al. [37] have given the detailed deduction process on how to calculate the refracted direction of the white light using the Snell law. While considering the monochromatic light, the same equation is applied to calculate the refracted ray except that the refractive index at the individual wavelength is used rather than at the primary wavelength (587.6 nm). The refractive ray can be obtained by the following equation:

$$\mathbf{T}(\lambda) = \frac{n(\lambda)}{n'(\lambda)}\mathbf{I}(\lambda) + \Gamma(\lambda)\mathbf{N}(\lambda), \tag{1}$$

where $\mathbf{I}(\lambda)$ and $\mathbf{T}(\lambda)$ are the unit vectors of the incident and refracted monochromatic rays at certain wavelength λ, respectively, $\mathbf{N}(\lambda)$ is the unit vector of the normal at the intersection between the incident ray and the lens surface, $n(\lambda)$ and $n'(\lambda)$ are the refractive indices of the materials at both sides of the lens surface boundary for the wavelength λ respectively, and $\Gamma(\lambda)$ is called partial derivative. All these quantities of this formula are dependent on wavelengths due to the lens dispersion. When the surface is a mirror, the incident ray will be reflected and the dispersion disappears. Reflection can be consider as a special situation of refraction with, and the reflected ray can be denoted as

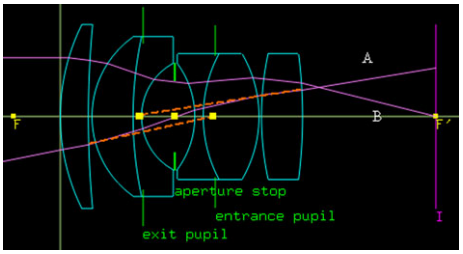

Fig. 8 Determination of entrance pupil and exit pupil. A ray through the center of the aperture (on the optical axis) is bound to penetrate the center of both pupils (also on the optical axis)

$$\mathbf{T} = -\mathbf{I} + 2(\mathbf{I} \cdot \mathbf{N})\mathbf{N}. \tag{2}$$

Equations (1) and (2) can be used to calculate the direction of the refracted or reflected ray in general sequential dispersive ray tracing algorithm inside a lens system.

5.3 Determination of pupils

Entrance pupil and exit pupil are fairly helpful for efficiently tracing rays through a lens system, as stated further in Sect. 6.1. Therefore, calculating the entrance pupil and exit pupil in a lens system, including their axial positions and sizes, is essential. Kolb et al. [12] presented an algorithm for finding the exit pupil using its imaging relationship with the aperture stop. Their algorithm assumes that the aperture stop is unknown, and thus needs to find the aperture stop at first. In fact, the aperture stop in the lens description is specified in advance, i.e. lens description tables of Fig. 9. Based on this observation and the conjugate characteristic among the aperture stop and its pupils, we propose a more easily implemented algorithm for locating the pupils in a lens system and calculating their size [37]. This algorithm can be divided into two stages: firstly, the positions of the pupils are determined by tracing two opposite rays emanating from the center of aperture stop, such as the ray path A in Fig. 8; secondly, the sizes of the pupils is calculated by iteratively searching the marginal ray that almost touches the rim of the aperture stop but passes through the entire lens system, such as the ray B in Fig. 8. The detailed process about our algorithm refers to previous work [37].

5.4 Dispersive ray tracing inside the lens system

For simulating the optical properties of physical lenses, a bidirectional sequential ray tracing (BSRT) approach [37] has been introduced and combined with traditional bidirectional ray tracing in the 3D scene. However, this approach cannot model the chromatic aberration phenomenon in lens systems. A naïve, direct modification on BSRT is to extend it by introducing the dispersion equations. Namely, when a

Algorithm 1 Dispersive sequential ray tracing

```
for every lens surface S_i of a lens system L do
  for every live ray R_j of the ray packet R do
    compute the intersection P_j of R_j and S_i
    if P_j is beyond aperture of the element then
      the ray R_j is marked as dead
    else
      compute the normal N_j of S_i at P_j
      compute the refracted (reflected) ray T_j using N_j and (1) and (2)
      update the ray R_j according to P_j and T_j
    end if
  end for
end for
```

monochromatic ray enters into the lens system, the refractive indices of all the lens materials for current wavelength in the lens system are updated using the dispersion equations, which take at this wavelength as the input parameter. Unfortunately, this naïve implementation is inefficient, as demonstrated later in Sect. 7.2. Inspired by the spread ray technique proposed by Yuan [38], we present a dispersive bidirectional sequential ray tracing (DBSRT) approach for modeling lens dispersion. The basic idea is to trace multiple rays of different wavelengths for improving efficiency of spectral rendering, which is later explained in discussing spectral rendering in Sect. 6. The detailed process of our method is described in Algorithm 1, where a packet of rays, $R_1, \ldots, R_k$, corresponds to k different wavelengths and comes from either the image plane or the 3D scene. Each of them has either of two states, live or dead, which indicate whether the ray has been blocked by the lens system in the successive tracing, and all the rays are live at the initialization stage.

6 Spectral rendering

6.1 Sampling lens model

Integrating our realistic lens model into a general ray tracer requires careful consideration on how to sample our lens model, mainly relating to placement of image and lens samples. Taking the path tracer as an example, the main problem involves how to generate a new camera ray which enters into the 3D scene through the lens model. A direct and naïve solution for this problem is to place an image sample point on the image plane and a lens sample point on the rear lens closest to the image plane, and then connect this pair of sample points to produce a new camera ray for further ray tracing through the lens model and scene. However, this solution is fairly low in efficiency because majority of the generated camera rays that pass through the rear lens are blocked by the rims of the successive lens elements, and eventually cannot pass through the lens system, which is illustrated in the profile view of the first lens of Fig. 9.

In order to improve efficiency of ray tracing, we place the lens sample on the entrance or exit pupils according to the optical properties of the aperture stop and its pupils, already explained in Sect. 3.1. Therefore, generating camera rays between the image plane (object plane) and exit pupil (entrance pupil) can improve efficiency of ray tracing, especially when the diameter of the aperture stop is small compared to the other apertures of the lens system, as illustrated in the profile view of the second and third lenses of Fig. 9.

6.2 Spectral ray tracing approach

Spectral rendering is essential for correctly modeling the specular dispersion [4]. A direct approach is the *single-wavelength* scheme, which generates the light path dependent on a randomly chosen wavelength. However it is inefficient because only single wavelength of light radiance is carried on each light path with high computational costs. Fortunately, an efficient, sparse direct sampling technique, stratified wavelength cluster (SWC), proposed by Evans and McCool [5], can be adapted to alleviate the above problem. Its basic idea is to firstly split the visual spectrum into K non-overlapped subregions,

$$\begin{cases} S_i = [\lambda_{\min} + i \cdot \Delta\lambda, \lambda_{\min} + (i+1) \cdot \Delta\lambda], \\ \Delta\lambda = (\lambda_{\max} - \lambda_{\min})/K, \\ i \in \{0, 1, \ldots, K-1\}, \end{cases} \tag{3}$$

where $\lambda_{\min}$ and $\lambda_{\max}$ are the up and lower bounds of the visual spectrum range. Then randomly choosing a wavelength λ_i from each subregion S_i, combining all the random wavelengths, $\lambda_0, \lambda_1, \ldots, \lambda_{K-1}$, finally forms a stratified wavelength cluster. In practice, for easy implementation and rendering efficiency, rather than generating a cluster of K stratified wavelengths by K random numbers, we use a single random number to uniformly dither all subregions to obtain a wavelength cluster.

Based on this technique, when tracing rays in our lens model and the 3D scene, each generated light path carries a bundle of wavelengths, not a single wavelength. When the specular refraction occurs, two different strategies are provided, namely (*splitting*) and (*degradation*). For the first strategy, the cluster is split into several separate light paths, but if using the other one, the cluster degrades into a single-wavelength light path by discarding all other wavelengths. The overall efficiency of this technique is fairly high since the fraction of clusters that need to be split or degraded in a typical scene is low. In addition, the specular dispersion tends to decrease the source color variance and offset the increased amortized cost of generating each path.

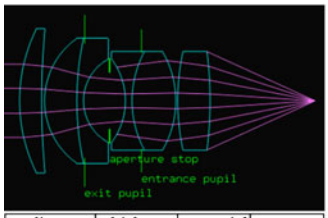

radius	thickness	material	aperture
85.500	11.600	LAF2	76.0
408.330	1.500	Air	76.0
40.350	17.000	SK55	66.0
156.050	3.500	FN11	66.0
25.050	13.700	Air	44.0
0.000	8.300	Air	42.6
-36.800	3.500	SF8	44.0
55.000	23.000	LAF2	52.0
-51.500	1.000	Air	52.0
123.500	17.000	LAF2	52.0
-204.960	0.000	Air	52.0

(a) F/1.35

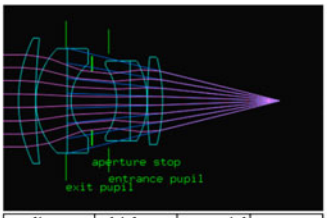

radius	thickness	material	aperture
75.050	9.000	LAF3	66.0
270.700	0.100	Air	66.0
39.270	16.510	BAF11	55.0
0.000	2.000	SF5	55.0
25.650	10.990	Air	39.0
0.000	13.000	Air	37.2
-31.870	7.030	SF5	37.0
0.000	8.980	LAF3	42.0
-43.510	0.100	Air	42.0
221.140	7.980	BAF11	46.0
-88.790	0.000	Air	46.0

(b) F/1.7

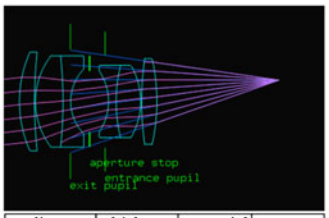

radius	thickness	material	aperture
63.900	7.900	SK8	52.0
240.300	0.500	Air	52.0
39.500	14.500	SK10	48.0
-220.500	4.000	F15	48.0
24.500	9.950	Air	34.0
0.000	9.950	Air	31.8
-28.700	4.000	F15	32.0
78.800	12.900	SK10	38.0
-37.900	0.500	Air	38.0
161.900	8.000	SK10	45.0
-103.200	0.000	Air	45.0

(c) F/2.0

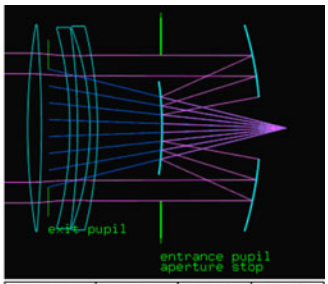

radius	thickness	material	aperture
212.834	4.463	UBK7	33.3
-390.476	9.174	Air	33.3
-125.482	2.480	UBK7	32.5
-231.298	3.967	Air	32.5
-91.834	2.480	UBK7	32.5
-133.883	20.400	Air	32.9
0.0	32.047	Air	33.1
-111.690	31.661	Mirror	33.2
-111.690	39.925	Mirror	15.0

(d) F/1.5

Fig. 9 Tabular descriptions and profile views of three double Gauss lenses and a catadioptric telephoto lens with the same focal length 100 mm [25]. In this paper, the lenses are labeled with their F stops, which are F/1.35, F/1.4, F/2.0, and F/1.5, respectively, and the last lens is a catadioptric lens. Each row in the tables describes a lens surface. Surfaces are listed in order from front to rear, with basic measurement unit in millimeters. The first column gives the signed radius of a spherical surface; if 0.0 is given, the surface is planar. A positive radius indicates a surface that is convex when viewed from the front of the lens, while a negative radius indicates a concave surface. The next entry is thickness, which measures the distance from this surface to the next surface along the optical axis. Following that is the material between the surface and the next surface. The last entry is the diameter of the aperture of the surface. The row with a radius of 0.0 and air at both sides of the surface signifies an adjustable diaphragm, namely the aperture stop

For the 3D scene, the degradation strategy works better than the other one because the separate tracing in a complex scene for each wavelength of a cluster increases the implementation complexity and computational costs. In the other way, the simplicity and regularity of the lens geometry supports efficient, parallel ray tracing of several light paths. Therefore, the splitting strategy is the better option for the dispersion of our lens model. Motivated by these observations, we propose a novel, *hybrid* scheme to handle different dispersions along the light path. Our scheme adapts the degradation strategy to handle the dispersion in the 3D scene, and the other one for the lens model. Combination of both strategies can greatly improve rendering performance, and the overview of our spectral rendering scheme is illustrated Fig. 10.

In this paper, we only consider how to model the lens dispersion rather than the common dispersion in the 3D scene, and thus assume that the scene is diffuse or barely specular. Given a non-dispersive lens model, the degradation strategy for the scene works very well and greatly improves the rendering efficiency. However, our lens model features the dispersion characteristic due to the presence of transparent materials, and thus dispersion always occurs when light rays traverse the lens model. As a result, this strategy degenerates to simple *single-wavelength* strategy. For solving this problem caused by our dispersive lens model, we defer the spectral ray tracing process inside the lens system until the ray tracing in the 3D scene is finished, and then different strategies are used at two stages.

Furthermore, we modify a widely used light transport algorithm, bidirectional path tracing [30], to incorporate the SWC technique and in particular discuss some special treatments to achieve correct integration between our lens model and this algorithm. Before using this algorithm to generate the camera and light sub-paths, we firstly produce a spectrum wavelength cluster perturbed at random. Notice that each pair of camera and light sub-paths must carry the same spectrum wavelength cluster for correct connection.

Camera sub-path: If the starting vertex of the camera sub-path is placed on the exit pupil, direct connection between this vertex and the light sub-path will be difficult because of the block of the lens model between them. Therefore, this vertex will be generated from the entrance pupil for easily obtaining the successive vertex or joining with the corresponding light sub-path. Based on this idea, we exploit the object plane, the conjugate plane of the image plane in the object space, and the entrance pupil to generate a ray shooting into the scene. *Light sub-path*: The light sub-path is generated like the traditional bidirectional path tracing, and no special cases are handled except that the SWC technique is used during the generation process. *Sub-path connection*: After both sub-paths are created, they are connected like the traditional bidirectional path tracing. Subsequently, the spectral ray tracing inside the lens model is executed to obtain multiple pixel positions on the image plane where the

connected ray path contributes its radiance. Exceptionally, if the camera sub-path contains only one vertex, a new ray starting on the entrance pupil is generated.

7 Results and discussion

Based on proposed dispersive lens model and spectral rendering approach, we have produced a variety of realistic and artistic bokeh effects caused by lens stops and lens aberrations, and all results were rendered on a workstation with Intel Xeon 5450 3.0G and main-memory of 4 GB. Figure 9 lists the prescriptions and 2D profile views of four lenses used in the following rendering experiments, and the apertures of the lenses are set to their adjustable maximum values for better capturing bokeh effects.

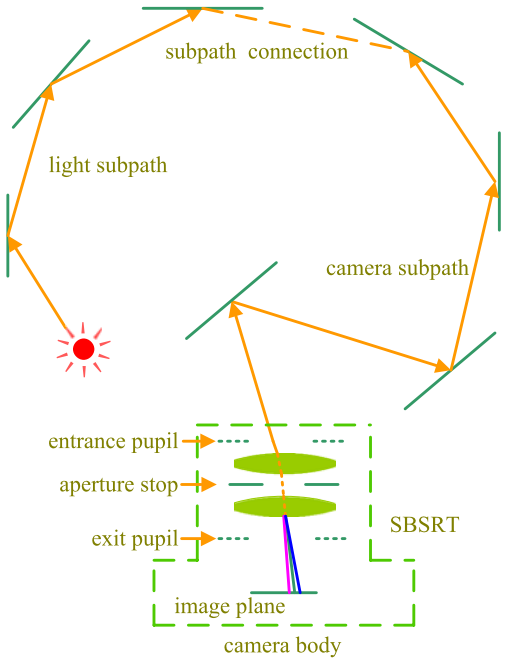

Fig. 10 Spectral rendering framework for integrating our lens model with the bidirectional ray tracing approach

7.1 Examples

Figure 11 is a simple scene composed of a row of glossy balls, different bokeh effects are generated by using four lenses at five different focal distances, and the shape of the aperture stop is circular. For the central balls in each row, their highlights have circular COCs like the aperture stop. When de-focused, they feature various intensity distributions within COCs, which are dependent on the spherical and chromatic aberrations of the lenses used. These distribution patterns are diverse, such as a bright core surrounded by a dark halo, a dark core with a bright halo, or other more complex forms. Notice that the donut-shape COCs in Fig. 11(d) appear due to block of rays by mirror elements of the catadioptric lens F/1.5. In Fig. 11(a)–(c), we can also observe that all COCs are colorful, which are caused by the chromatic aberration of physical lenses. However, in Fig. 11(d), the COCs are gray and intensity distributions are uniform because of mirror elements of the catadioptric telephoto lens. In lens design field, mirror elements are usually used to eliminate or reduce the spherical and chromatic aberrations existing in physical lenses [25].

However, for these more peripheral balls, their COCs start to become non-circular and feature various shapes, such elliptical, cometic, or other more complex forms, and the light intensity distributions within these COCs are more complex than the central ones. The variation of the COC shape and its intensity distribution is affected by vignetting stop, coma, astigmatism and field curvature together.

Figure 12 displays a variety of bokeh effects by a slightly complex chess scene, where we see various colorful bokeh effects in both foreground and background of each image due to co-influence of multiple kinds of lens aberrations. In Fig. 12(a)–(c), observe that the chromatic aberration only affects the appearance of the highlights in the images, while other parts of the images are free from the chromatic aberration. This phenomenon is consistent with the explanation in Sect. 4.2. In Fig. 12(d), the chromatic bokeh effects disappear because of anti-chromatic characteristic of the catadioptric telephoto F/1.5.

Figure 13 illustrates a variety of bokeh effect using the same chess scene as Fig. 12, but these effects are affected

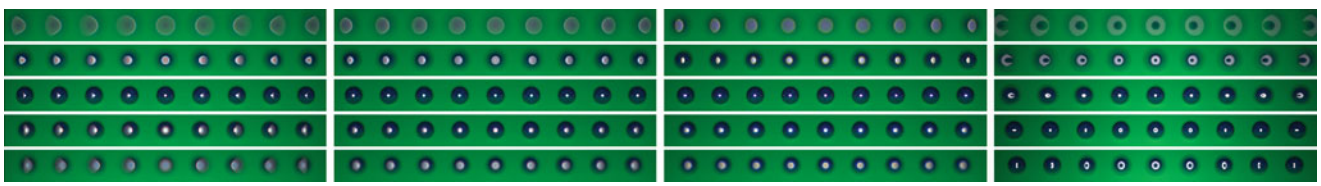

(a) F/1.35 (b) F/1.7 (c) F/2.0 (d) F/1.5

Fig. 11 A scene of a row of balls on a green background for showing bokeh effects using three double Gauss lenses, F/1.35, F/1.7, and F/2.0 and one catadioptric telephoto lens, F/1.5 at different focal distances. Note that the changes of bokeh patterns from center to edge due the focal distances and lens aberrations

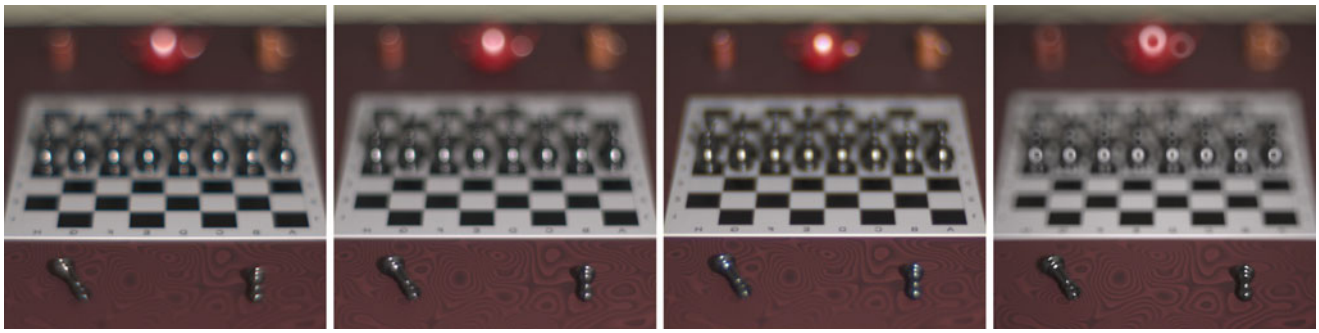

(a) F/1.35 (b) F/1.7 (c) F/2.0 (d) F/1.5

Fig. 12 A chess scene for showing bokeh effects using three double Gauss lenses, F/1.35, F/1.7, and F/2.0 and one catadioptric telephoto lens, F/1.5

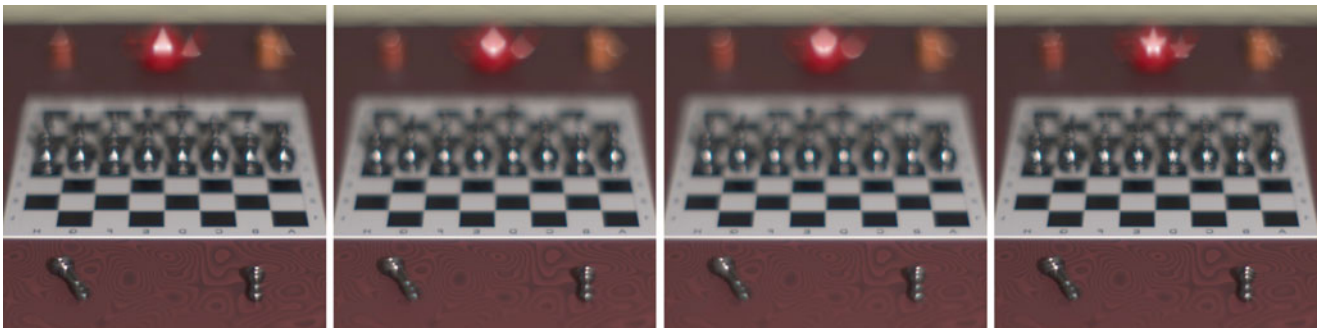

(a) Triangular (b) Rectangular (c) Pentagonal (d) Starry

Fig. 13 Bokeh effects due to different shapes of lens stops, triangular, rectangular, pentagonal, and starry, respectively, and the lens used is double Gauss lens F/1.35

Fig. 14 A bubble scene for showing bokeh effects. The lens used is double Gauss F/1.35, and the apertures are circular, triangular, rectangular, and starry, respectively

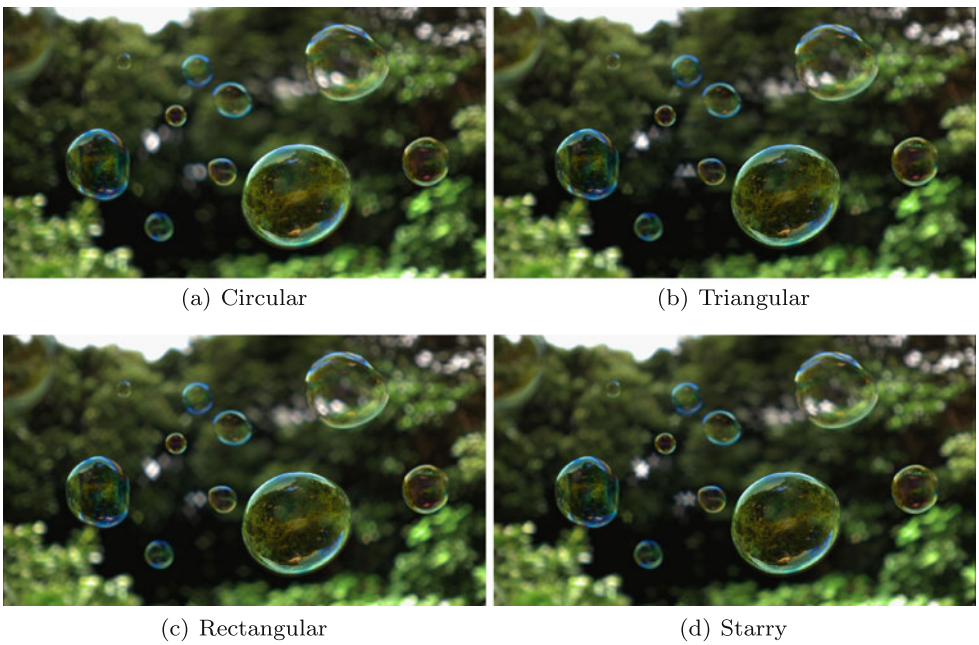

(a) Circular (b) Triangular

(c) Rectangular (d) Starry

by lens stops and lens aberrations together. The lens used is double Gauss lens F/1.35. From Fig. 13(a) to Fig. 13(d), the aperture shapes are triangular, rectangular, pentagonal, and starry, respectively. Notice that the bokeh shape in the middle is more similar to the shape of the aperture stop used, but the bokeh shape in the periphery is more complex due to in-

fluence of multiple kinds of lens aberrations. Figure 14 is a scene containing a few bubbles, plus an environment lighting using a texture image. These images illustrate various bokeh effects featuring intensely artistic sense.

7.2 Comparisons

Figure 15 compares our bokeh rendering method and the monochromatic one [37], which is so far the most accurate one for rendering bokeh effects. It is seen that the monochromatic one only produces gray bokeh effects, but ours is able to simulate chromatic bokeh effects caused by monochromatic and chromatic aberrations together. For verifying our method, we also did a real photograph experiment using a common digital camera, Cannon EOS 50D with F/1.4, shown in Fig. 16(a). From this figure, we clearly observe that these colorful bokehs are similar to that produced by our method. The lens used by our method is a wide-angle lens F/3.4 (Modern lens design [25], p. 358), which is consistent with the wide-angle properties of this digital camera. However, accurate comparisons between the images simulated by our method and the real photographs are fairly difficult because the detailed optical data of real camera lenses are unobtainable and 3D modeling for actual scenes captured in the photographs refers to another specialized field.

Figure 17 illustrates the visual comparison about our hybrid scheme and the single wavelength scheme. It is seen that our hybrid scheme produces less noise and sharper bokeh appearance than the single wavelength scheme. The images by both schemes were rendered with the same time: one hour and twenty-six minutes and the reference image was rendered with ninety-one hours and eighteen minutes. In order to give a quantitative measurement on both schemes, we compare our new hybrid scheme with the single wavelength scheme using two different image quality measurement methods: peak signal-to-noise ratio (PSNR) and structural similarity (SSIM) [34]. For both measurement methods, higher value or index indicates better image quality. We compare the images produced by both schemes with

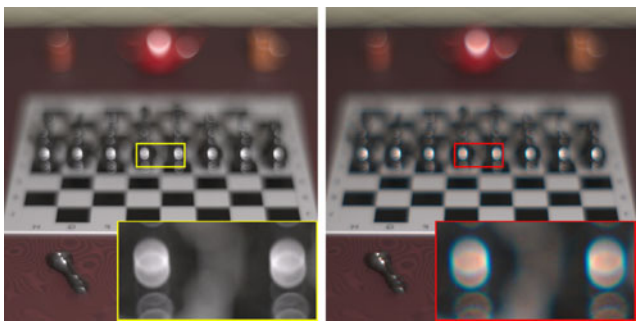

(a) Monochromatic (b) Ours

Fig. 15 Comparison between the monochromatic bokeh rendering method (**a**) and ours (**b**). Note that our method can produce colorful bokeh effect that the monochromatic one cannot

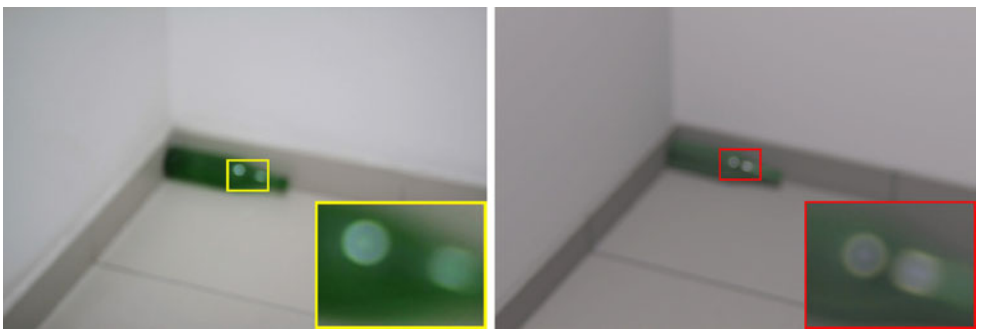

(a) Photograph (b) Ours

Fig. 16 Comparison between real photograph (**a**) and our method (**b**). To some extent, note that their similarity in intensity distributions and colorful fringes. The real photograph is captured using a real digital camera, Cannon EOS 50D with F/1.4

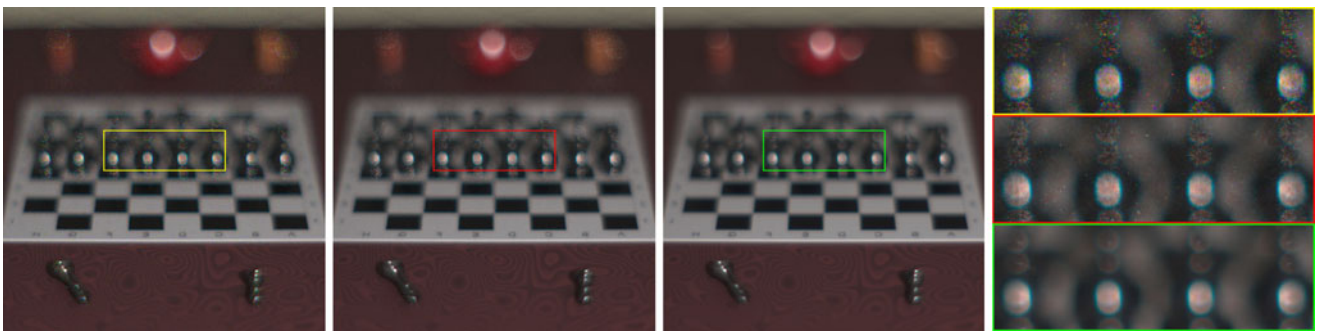

(a) Single-wavelength scheme (b) Our hybrid scheme (c) Reference (d) Closeup

Fig. 17 Comparison of rendering performance on single-wavelength scheme and our hybrid scheme with equal time (Lens used is F/1.35)

Table 1 Comparison of rendering performance on single wavelength scheme and our hybrid scheme using PSNR and SSIM. The time format is hour/minute

	Time	1:26	2:23	5:13	25:51
PSNR(dB)	Single	39.47	40.98	43.29	46.90
	Ours	40.82	42.38	45.21	50.78
SSIM	Single	0.9634	0.9769	0.9882	0.9950
	Ours	0.9742	0.9843	0.9927	0.9981

the same rendering time, to the reference image, respectively. The PSNR values and SSIM indices under different rendering time for both schemes are listed in Table 1. Note that our hybrid scheme produces higher PSNR values and SSIM indices, which means that our hybrid scheme is more efficient and produces better image quality than the single wavelength scheme with the same rendering time.

8 Conclusion

We have presented a novel approach for simulating realistic spectral bokeh effects due to lens stops and aberrations. Bokeh effects depend on geometrical elements (lens stops) and optical factors (lens aberrations) of complex lens systems, which mainly influence their shape and light intensity distribution of bokeh. In order to simulate these lens-related effects, we have proposed two important techniques: an accurate dispersive camera lens model and an efficient spectral rendering scheme, which have been demonstrated by multiple rendering experiments and comparisons.

Despite high accuracy of our lens model, some other optical effects are still not taken into account, such as unwanted reflections on the inner lens surfaces. Therefore, in the future, we intend to model unwanted reflections to refine our lens model. Another important aspect of the future work is to accelerate rendering of bokeh effect, for instance, reducing average samples per pixel by combining bokeh blur characteristic with adaptive rendering techniques [7, 21, 26], and accelerating rendering of bokeh pattern by expanding metropolis sampling techniques [10, 31] based on bokeh's highlight characteristic. In addition, our lens model can also be introduced into real-time rendering for achieving more realistic lens effect than pin-hole model or thin lens model, and fortunately, recently released ray tracing engine OptiX [22], developed by NVIDIA, provides a suitable platform for implementing our lens model.

Acknowledgements We thank the LuxRender community and anonymous provider for the chess and bubble scenes. This work was partly supported by the National High-Tech Research and Development Plan of China (Grant No. 2009AA01Z303).

References

1. Ang, T.: Dictionary of Photography and Digital Imaging: The Essential Reference for the Modern Photographer. Watson-Guptill, New York (2002)
2. Born, M., Wolf, E.: Principles of Optics, 7th edn. Cambridge University Press, Cambridge (1999)
3. Buhler, J., Wexler, D.: A phenomenological model for bokeh rendering. In: Computer Graphics Proceedings, Annual Conference Series, ACM SIGGRAPH Abstracts and Applications, San Antonio, p. 142 (2002)
4. Devlin, K., Chalmers, A., Wilkie, A., Purgathofer, W.: Tone reproduction and physically based spectral rendering. Eurographics 2002: State of the Art Reports, pp. 101–123 (2002)
5. Evans, G.F., McCool, M.D.: Stratified wavelength clusters for efficient spectral Monte Carlo rendering. In: Graphics Interface, pp. 42–49 (1999)
6. Fischer, R.E., Tadic-Galeb, B., Yoder, P.R.: Optical System Design, 2nd edn. McGraw-Hill, New York (2008)
7. Hachisuka, T., Jarosz, W., Weistroffer, R.P., Dale, K.: Multidimensional adaptive sampling and reconstruction for ray tracing. ACM Trans. Graph. (Proc. ACM SIGGRAPH Conf.) **27**(3), 33 (2008)
8. Haeberli, P., Akeley, K.: The accumulation buffer: hardware support for high-quality rendering. In: Computer Graphics Proceedings, Annual Conference Series, ACM SIGGRAPH, Dallas, pp. 309–318 (1990)
9. Kass, M., Lefohn, A., Owens, J.: Interactive depth of field using simulated diffusion on a gpu. Technical report, Pixar Animation Studios (2006)
10. Kelemen, C., Szirmay-Kalos, L., Antal, G., Csonka, F.: A simple and robust mutation strategy for the metropolis light transport algorithm. Comput. Graph. Forum **21**(3), 1–10 (2002)
11. Kodama, K., Mo, H., Kubota, A.: Virtual bokeh generation from a single system of lenses. In: Computer Graphics Proceedings, Annual Conference Series, ACM SIGGRAPH Research Posters, Boston, p. 77 (2006)
12. Kolb, C., Mitchell, D., Hanrahan, P.: A realistic camera model for computer graphics. In: Computer Graphics Proceedings, Annual Conference Series, ACM SIGGRAPH, Los Angeles, pp. 317–324 (1995)
13. Kosloff, T.J., Tao, M.W., Barsky, B.A.: Depth of field postprocessing for layered scenes using constant-time rectangle spreading. In: Proceedings of Graphics Interface, Kelowna, pp. 39–46 (2009)
14. Kraus, M., Strengert, M.: Depth-of-field rendering by pyramidal image processing. Computer Graphics Forum **26**(3) (2007)
15. Laikin, M.: Lens Design, 3th edn. Marcel Dekker, New York (2001)
16. Lanman, D., Raskar, R., Taubin, G.: Modeling and synthesis of aperture effects in cameras. In: Proceedings of International Symposium on Computational Aesthetics in Graphics, Visualization, and Imaging, Lisbon, pp. 102–106 (2008)
17. Lee, S., Eisemann, E., Seidel, H.P.: Depth-of-field rendering with multiview synthesis. ACM Trans. Graph. (Proc. ACM SIGGRAPH Asia Conf.) **28**(5), 1–6 (2009)
18. Lee, S., Eisemann, E., Seidel, H.P.: Real-time lens blur effects and focus control. ACM Trans. Graph. (Proc. ACM SIGGRAPH Conf.) **29**(3), 1–7 (2010)
19. Lee, S., Kim, G.J., Choi, S.: Real-time depth-of-field rendering using point splatting on per-pixel layers. Comput. Graph. Forum **27**(7), 1955–1962 (2008)
20. Merklinger, H.M.: A technical view of bokeh. Photo Tech. **18**(3), 37–41 (1997)
21. Overbeck, R.S., Donner, C., Ramamoorthi, R.: Adaptive wavelet rendering. ACM Trans. Graph. (Proc. ACM SIGGRAPH Asia Conf.) **28**(5), 140 (2009)

22. Parker, S.G., Bigler, J., Dietrich, A., Friedrich, H., Hoberock, J., Luebke, D., McAllister, D., McGuire, M., Morley, K., Robison, A., Stich, M.: Optix: A general purpose ray tracing engine. In: ACM Transactions on Graphics (Proceedings of the SIGGRAPH conference) (2010)
23. Potmesil, M., Chakravarty, I.: A lens and aperture camera model for synthetic image generation. In: Computer Graphics Proceedings, Annual Conference Series, ACM SIGGRAPH, Dallas, pp. 297–305 (1981)
24. Riguer, G., Tatarchuk, N., Isidoro, J.: Real-time depth of field simulation. In: Engel, W.F. (ed.) Shader X2: Shader Programming Tips and Tricks with DirectX 9, pp. 529–556. Wordware, Plano (2003)
25. Smith, W.J.: Modern Lens Design. McGraw Hill, New York (1992)
26. Soler, C., Subr, K., Durand, F., Holzschuch, N., Sillion, F.: Fourier depth of field. ACM Trans. Graph. **28**(2), 18 (2009)
27. Sun, Y., Fracchia, F.D., Drew, M.S.: Rendering light dispersion with a composite spectral model. In: International Conference on Color in Graphics and Image Processing (2000)
28. Sun, Y., Fracchia, F.D., Drew, M.S., Calvert, T.W.: A spectrally based framework for realistic image synthesis. Vis. Comput. **17**(7), 429–444 (2001)
29. Thomas, S.W.: Dispersive refraction in ray tracing. Vis. Comput. **2**(1), 3–8 (1986)
30. Veach, E.: Robust Monte Carlo methods for light transport simulation. Ph.D. thesis, Stanford University (1997)
31. Veach, E., Guibas, L.J.: Metropolis light transport. In: Computer Graphics Proceedings, Annual Conference Series, ACM SIGGRAPH, pp. 65–76 (1997)
32. van Walree, P.: Chromatic aberrations. http://toothwalker.org/optics/chromatic.html
33. van Walree, P.: Vignetting. http://toothwalker.org/optics/vignetting.html
34. Wang, Z., Bovik, A.C., Sheikh, H.R., Simoncelli, E.P.: Image quality assessment: From error visibility to structural similarity. IEEE Trans. Image Process. **13**(4), 600–612 (2004)
35. Wikipedia: Bokeh. http://en.wikipedia.org/wiki/Bokeh
36. Wikipedia: Dispersion (optics). http://en.wikipedia.org/wiki/Dispersion_(optics)
37. Wu, J., Zheng, C., Hu, X., Wang, Y., Zhang, L.: Realistic rendering of bokeh effect based on optical aberrations. Vis. Comput. **26**(6), 555–563 (2010)
38. Yuan, Y., Kunii, T.L., Inamoto, N., Sun, L.: Gemstonefire: adaptive dispersive ray tracing of polyhedrons. Vis. Comput. **4**(5), 259–270 (1988)
39. ZEMAX: Zemax: software for optical system design. www.zemax.com

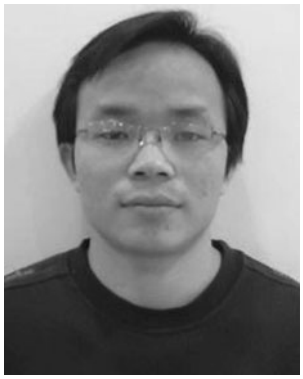

Jiaze Wu is a Ph.D. student in the National Key Laboratory of Integrated Information System Technology, Institute of Software, Chinese Academy of Sciences. He received his B.Sc. degree from Nankai University in 2005. His research interests include real-time rendering, realistic rendering, virtual reality, and optical simulation.

Changwen Zheng is a Professor in the National Key Laboratory of Integrated Information System Technology, Institute of Software, Chinese Academy of Sciences. He received his Ph.D. degree from Huazhong University of Science and Technology. His research interests include computer graphics, virtual reality, computer simulation, and artificial intelligence.

Xiaohui Hu is a Professor in the National Key Laboratory of Integrated Information System Technology, Institute of Software, Chinese Academy of Sciences. He received his Ph.D. degree from Beijing University of Aeronautics and Astronautics. His research interests include computer graphics, virtual reality, and computer simulation.

Fanjiang Xu is a Professor in the National Key Laboratory of Integrated Information System Technology, Institute of Software, Chinese Academy of Sciences. His research interests include computer graphics, virtual reality, and computer simulation.